Journal of Analysis and Testing (2024) 8:278–287
https://doi.org/10.1007/s41664-024-00298-y

ORIGINAL PAPER

Integrating Bimetallic Nanoparticles with Covalent Organic Frameworks as Multifunctional Nanozyme for Colorimetric Detection of Hydrogen Peroxide and Glutathione

Yuying Yuan[1] · Xiaoxue Xi[1] · Ting Bao[1] · Pingguan Bian[2] · Feng Pei[2] · Xiuhua Zhang[1] · Shengfu Wang[1] · Wei Wen[1]

Received: 31 December 2023 / Accepted: 29 January 2024 / Published online: 13 March 2024

Abstract
The controllable growth of metal nanoparticles on nanomaterials is becoming an effective strategy for developing nanocomposites with designated performance. Herein, a simple and mild strategy for the in situ growth of Pt–Pd bimetallic nanoparticles on covalent organic frameworks (COFs) to regulate the nanozyme activity was designed for colorimetric detection of hydrogen peroxide (H_2O_2) and glutathione (GSH). The COFs not only offer sufficient loading sites for the uniform dispersion of Pt–Pd bimetallic nanoparticles, but also increase the adsorption of substrate to promote the catalytic reaction. With the bimetallic synergistic effect of Pt–Pd nanoparticles, the prepared multifunctional nanozyme (Pt–Pd/COFs nanozyme) simultaneously exhibited superior peroxidase (POD)-like activity and oxidase (OXD)-like activity. Using the multifunctional nanozyme, a colorimetric sensing system was constructed for sensitive detection of H_2O_2 and GSH, with the wide linear ranges of 5–1000 μmol/L and 1–40 μmol/L, and the detection limits were 1.14 μmol/L and 0.43 μmol/L, respectively. It was successfully used for the detection of real samples in environmental water and serum, providing a simple method for disease diagnosis and environmental monitoring.

Keywords Pt–Pd/COFs nanozyme · Bimetallic synergistic effect · Peroxidase-like activity · Oxidase-like activity · H_2O_2 and GSH detection

1 Introduction

Nanozymes, a class of desirable nanomaterial with intrinsic enzyme-like activity, have become spotlight in the catalysis, energy and environmental protection fields [1–3]. Compared with natural enzymes, nanozymes hold the advantages including excellent environmental stability, controllable composition, low-cost and ease of synthesis [4–6]. Yan's group found that Fe_3O_4 nanoparticles possess excellent peroxidase-like activity in 2007 [7]. Subsequently, various nanomaterials have been reported to exhibit enzymes-like activities, such as noble metals, metal oxides [8–10], carbon-based nanomaterials [11], metal–organic frameworks [12, 13], single-atom materials [14, 15]. Among them, noble metal nanomaterials (Au, Pt, Pd, Ag) are favored by researchers due to their outstanding catalytic activity, adjustable composition and morphology [16, 17]. However, the uncontrolled size caused by aggregation and the insufficient adsorption sites for substrate still limit their catalytic activity. The controllable growth of noble metal nanoparticles on nanomaterials is an effective strategy to improve the catalytic performance [18, 19], which not only anchors nanoparticles to reduce aggregation, but also increases the adsorption sites of substrate to promote the catalytic reaction.

Covalent organic frameworks (COFs) are a novel type of organic porous polymer composed of organic units in the form of covalent interactions [20, 21]. Due to their good stability, low density, tunable pore size and large specific surface areas [22, 23], COFs have demonstrated to be outstanding nanocarriers for improving the dispersion

✉ Ting Bao
baoting@hubu.edu.cn

✉ Wei Wen
wenwei@hubu.edu.cn

[1] Collaborative Innovation Center for Advanced Organic Chemical Materials, Co-constructed by the Province and Ministry of Education Key Laboratory for the Synthesis and Application of Organic Functional Molecules, College of Chemistry and Chemical Engineering, Hubei University, Wuhan 430062, China

[2] Hubei Yihua Chemical Co., Ltd, Yichang 443000, China

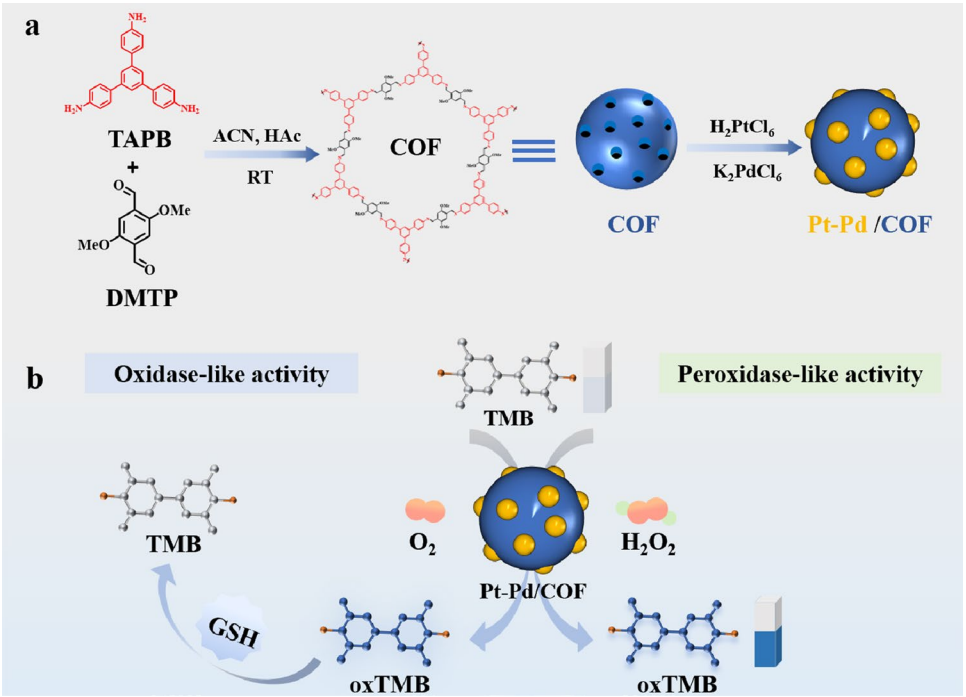

Scheme 1 **a** Synthesis of Pt–Pd/COFs nanozyme **b** Colorimetric sensing platform based on multifunctional Pt–Pd/COFs nanozyme: POD-like activity for H_2O_2 detection in TMB-H_2O_2 system; OXD-like activity for GSH detection in O_2–TMB system

and catalytic activity of metal nanoparticles [24–26]. Meanwhile, COFs hold unique molecular structure with pore space confinement effect, providing abundant anchor sites for limiting the size of noble metal nanoparticles. The strong interactions between the confined metal nanoparticles and COFs constructed by imine bonds can not only improve the stability of the active metal centers, but also enhance their catalytic activity [27]. Therefore, integrating nanoparticles with COFs provides a new paradigm to develop multifunctional nanozyme with designated performance.

Hydrogen peroxide (H_2O_2) is an important biomarker in the enzyme-catalyzed biochemical reactions, which plays a vital role in maintaining life activities. The abnormal changes of H_2O_2 concentration are closely related to the occurrence of different diseases including cardiovascular diseases and cancer [28]. Glutathione (GSH) is one of the most abundant sulfhydryl compounds in cells, which plays an essential role in maintaining physiological functions in human body. GSH can act as an antioxidant and free radical removal agent by binding to free radicals, facilitating the conversion of harmful toxins into harmless substrates and promoting their elimination from the body [29]. Therefore, it is crucial to monitor H_2O_2 and GSH levels for early diagnosis of disease. Currently, various methods have been proposed for GSH and H_2O_2 detection, including photoelectrochemistry [30], fluorescence [31], colorimetry [32, 33] and electrochemical biosensor [34]. Among these methods, colorimetric sensing platform possesses the advantages of simplicity, fast response and low-cost [35, 36], which facilitates visual detection by the naked eyes and can be used as a powerful tool for the detection of H_2O_2 and GSH.

In this work, we prepared a novel Pt–Pd/COFs nanozyme through a simple aldimine condensation reaction and in-situ reduction method. The COFs was synthesized with 1,3,5-tris(4-aminophenyl)benzene (TAPB) and 2,5-dimethoxyterephaldehyde (DMTP) as monomer, which provided abundant anchor sites for Pt–Pd bimetallic nanoparticles to enhance the catalytic activity and stability. With the synergistic effect of Pt–Pd bimetallic nanoparticles, the prepared multifunctional Pt–Pd/COFs nanozyme held superior peroxidase (POD)-like activity and oxidase (OXD)-like activity, which was used to construct colorimetric sensing platform for H_2O_2 and GSH detection (Scheme 1). The turn-on mechanism in the 3,3′,5,5′-tetramethylbenzidine (TMB)–H_2O_2 system was confirmed to the generated ·OH triggered TMB oxidation process, which realized the detection of H_2O_2. In addition, the turn-off mechanism in the O_2–TMB system was ascribed to the presence of GSH, leading to the reduction of oxidized-TMB and achieving quantitative detection of GSH. Importantly, the Pt–Pd/COFs nanozyme achieved efficient detection of H_2O_2 and GSH in complex samples, holding promising applications in disease diagnosis and environmental monitoring.

2 Experimental

2.1 Chemical Reagents and Instruments

The information of chemical reagents and instrumentations were shown in the supporting information.

2.2 Synthesis of Pt–Pd/COFs Nanozyme

The COFs were synthesized according to the reported literature [37] and the details were shown in the supporting information. The obtained COFs (4.0 mg) were dissolved in 3.0 mL methanol with the addition of 1.0 mL $H_2PtCl_6{\cdot}H_2O$ (6.0 mmol/L) and K_2PdCl_4 (6.0 mmol/L) to deposit bimetallic precursors into COFs by freeze-drying method [38], and then redispersed in 5 mL MeOH/H_2O solution (3:2, *V*/*V*) under vigorous stirring. Subsequently, 2.0 mL $NaBH_4$ (0.25 mol/L) was introduced into the above solution and reacted for 24 h. After centrifugation and washed with ethanol and ultrapure water, the products were redispersed in 2 mL ultrapure water for further utilization. Pt/COFs and Pd/COFs were prepared without adding platinum precursor or palladium precursor under the same reaction conditions.

2.3 Kinetic Assay of Pt–Pd/COFs Nanozyme

The steady-state dynamics assay of Pt–Pd/COFs nanozyme was examined with various concentrations of TMB (0.2–0.7 mmol/L) or H_2O_2 (0.2–0.7 mmol/L). Total volume of final solution was 3.0 mL. The absorbance at 652 nm (A_{652}) was recorded through the kinetic mode of UV–vis spectrometer. The kinetic data were fitted with a typical Michaelis–Menten curve. The Michaelis–Menten equation is as follows:

$$\frac{1}{V} = \left(\frac{K_m}{V_{max}}\right) \times \left(\frac{1}{[S]}\right) + \frac{1}{V_{max}} \quad (1)$$

where [*S*] is the substrate concentration (TMB or H_2O_2), V_{max} is the maximum reaction velocity speed, K_m represents the Michaelis constant.

2.4 Evaluation of Enzyme-Like Activities of Pt–Pd/COFs Nanozyme

The catalytic mechanism of multifunctional Pt–Pd/COFs nanozyme was also discussed. Firstly, the 1,4-benzoquinone (PBQ) was selected as trapping agent of $O_2^{\cdot-}$. Pt–Pd/COFs (20 μg/mL), TMB (0.3 mmol/L) and PBQ (1 mmol/L) were added into NaAc–HAc buffer, and the final volume of reaction solution was 3.0 mL. Then the A_{652} of the solution was recorded. Furthermore, the formation of ·OH was explored with the assistance of terephthalic acid (PTA), which can react with ·OH and generate the product with strongly fluorescence at 425 nm. In which, Pt–Pd/COFs (2.5 μg/mL), TMB (0.3 mmol/L) and PTA (0.5 mmol/L) were added into NaAc-HAc buffer and the total volume of solution was 3.0 mL, and the absorbance values at 425 nm were recorded.

2.5 Colorimetric Detection of H_2O_2 and GSH

Pt–Pd/COFs nanozyme exhibited catalytic activity towards H_2O_2–TMB system and O_2–TMB system, due to excellent POD-like activity and OXD-like activity. Therefore, a turn-on colorimetric assay based on TMB–H_2O_2–Pt–Pd/COFs nanozyme system was developed for the detection of H_2O_2. For H_2O_2 sensing, 30 μL TMB (0.3 mmol/L), 10 μL Pt–Pd/COFs nanozyme (2.5 μg/mL) and 100 μL H_2O_2 with various concentrations were added into NaAc-HAc buffer with the final reaction volume of 3.0 mL. After incubation for 5 min, the final reaction system was measured by a UV–Vis spectrometer.

Taking advantage of the reducibility of GSH, a turn-off colorimetric platform based on TMB–O_2–Pt–Pd/COFs nanozyme system was constructed for GSH detection. In brief, 50 μL GSH solution with different concentrations, 0.3 mmol/L TMB and 20 μg/mL Pt–Pd/COFs nanozyme were added into NaAc-HAc buffer and incubated for 20 min. Then, A_{652} of the solution was recorded.

2.6 Colorimetric Detection of H_2O_2 and GSH in Practical Samples

To evaluate the practical application capability of the Pt–Pd/COFs nanozyme, the recovery experiments in serum sample and environmental water were conducted. The serum was diluted 100-fold with NaAc–HAc buffer and the GSH with different concentrations (20 μmol/L, 30 μmol/L, 40 μmol/L) was added. Similarly, the standard H_2O_2 with different concentrations (200 μmol/L, 500 μmol/L, 1000 μmol/L) was added into environmental water. Finally, the prepared samples were detected by the colorimetric platform based on Pt–Pd/COFs nanozyme.

3 Results and Discussion

3.1 Characterization of Materials

The COFs were synthesized by Schiff-base condensation reaction with TAPB and DMTP as the reaction monomers, and Pt–Pd/COFs nanozyme was synthesized through in situ reduction method. The size and morphology of COFs and Pt–Pd/COFs were analyzed by scanning electron microscope

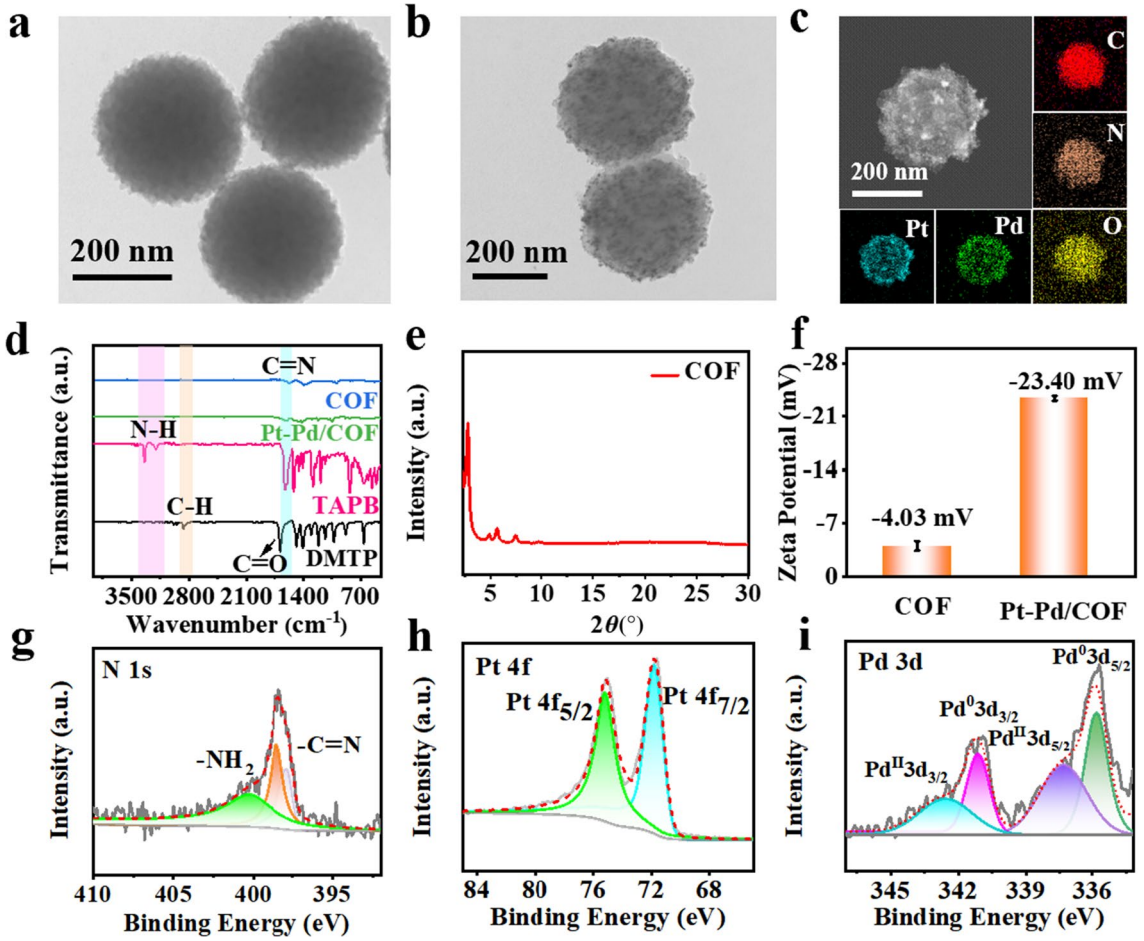

Fig. 1 TEM images of **a** COFs and **b** Pt–Pd/COFs. **c** EDS element mapping of Pt–Pd/COFs. **d** FT-IR spectra of COFs, Pt–Pd/COFs, TAPB and DMTP. **e** XRD pattern of COFs. **f** Zeta potentials of COFs and Pt–Pd/COFs. High-resolution XPS spectra of **g** N 1s, **h** Pt 4f and **i** Pd 3d

(SEM) and transmission electron microscope (TEM). As shown in Fig. 1a and Fig. S1, the prepared COFs exhibited a spherical shape structure with the particle size about 200 nm. Besides, the uniform distribution of Pt–Pd bimetallic nanoparticles could be observed on Pt–Pd/COFs nanozyme, and the anchor of the bimetallic nanoparticles did not affect the structure of COFs (Fig. 1b and Fig. S2). Furthermore, the elemental mapping of Pt–Pd/COFs was also conducted to reveal the element composition and distribution. Figure 1c illustrated the homogeneous dispersion of Pt–Pd bimetallic nanoparticles on COFs, demonstrating that Pt–Pd bimetallic nanoparticles were successfully deposited on COFs. These results revealed the successful formation of Pt–Pd/COFs nanozyme. In addition, Fourier transform infrared spectroscopy (FT-IR) of DMTP, TAPB, COFs and Pt–Pd/COFs were also carried out to verify the composition of chemical bonds. As shown in Fig. 1d, a distinct peak at 1675 cm^{-1} was observed, which belonged to the tensile vibration of C=O bonds of DMTP, and the characteristic peak at 2759 cm^{-1} could be associated with the vibration of C–H bond in the –CHO groups. The peaks of TAPB at 3226 cm^{-1} and 3343 cm^{-1} were attributed to the stretching bond of N–H. The disappearance of -NH_2 (3343 cm^{-1}) and –CHO (1675 cm^{-1}) peaks for the monomers and the appearance of a new peak (1586 cm^{-1}) for imine bonds suggested the successful occurrence of condensation reaction between –NH_2 and –CHO groups. Meanwhile, the crystallinity of COFs was further characterized by powder X-ray diffraction (PXRD). As observed in Fig. 1e, a prominent peak at 2.80° and a series of weak peaks (4.78°, 5.60°, 7.44°, 9.71° were observed, corresponding to the (100), (110), (200), (210), (220) crystal planes respectively, which proved the successfully formation of high crystalline COFs [37]. Then the formation of Pt–Pd/COFs nanozyme was investigated by zeta potential. As shown in Fig. 1f, the zeta potential of COFs changed from − 4.03 to − 23.40 mV after modified with Pt–Pd bimetallic nanoparticles. X-ray photoelectron spectroscopy (XPS) patterns of the COFs and Pt–Pd/COFs were presented in Fig. S3. The peaks of C 1s, O 1s and N 1s displayed in the XPS pattern of COFs. After loaded with

Pt–Pd bimetallic nanoparticles, the peaks of Pt 4f and Pd 3d could be observed in the XPS pattern of Pt–Pd/COFs. The peaks at 398.60 eV and 400.30 eV were shown in the N 1s spectrum (Fig. 1g), which were associated with C=N and $–NH_2$ [39]. The appearance of C=N bonds confirmed the successful preparation of TAPB-DMTP COFs by Schiff-based condensation reaction. As shown in Fig. 1h, a pair of peaks at 71.3 eV and 74.4 eV could be assigned to Pt $4f_{7/2}$ and Pt $4f_{5/2}$, indicating that Pt element was mainly zero-valence state in the Pt–Pd/COFs. As shown in Fig. 1i, the peaks at 337.3 eV and 342.6 eV could be ascribed to the $3d_{3/2}$ and $3d_{5/2}$ orbitals of Pd, respectively. In addition, the peaks at 341.1 eV and 337.3 eV represented the $3d_{3/2}$ and $3d_{5/2}$ orbitals of PdO [40]. The experimental results demonstrated the successful preparation of Pt–Pd/COFs nanozyme.

3.2 Kinetic Assay of Pt–Pd/COFs Nanozyme

To explore the catalytic efficiency of Pt–Pd/COFs nanozyme, the steady-state kinetic was studied with TMB (Fig. 2a,c) and H_2O_2 (Fig. 2b,d) as substrates, respectively. Based on the typical Michaelis–Menten kinetics Eq. (1), where V_{max} means the maximum velocity and K_m is the Michaelis–Menten constant, typically, a smaller K_m represents stronger affinity between the enzyme and substrate, the K_m and V_{max} with TMB as substrate were 1.12 mmol/L and 34.15×10^{-8} (mol/L)/s, respectively, and the K_m and V_{max} for H_2O_2 were 0.32 mmol/L and 19.27×10^{-8} (mol/L)/s, respectively, indicating that Pt–Pd/COFs nanozyme had high affinity for H_2O_2. The novel Pt–Pd/COFs nanozyme had high V_{max} and low K_m values, which was associated with the outstanding catalytic activity of bimetallic nanoparticles and the high loading capacity of COFs.

3.3 The Catalytic Mechanism of Pt–Pd/COFs Nanozyme

To check the catalytic activity of Pt–Pd/COFs nanozyme towards the H_2O_2–TMB system, POD-like activity of COFs, Pt/COFs, Pd/COFs, Pt–Pd/COFs were investigated, respectively. In Fig. 3a, b, the negligible absorption peak was observed in TMB–H_2O_2 system when no material was added or only COFs were present. In contrast, the reaction system containing Pt–Pd/COFs appeared stronger absorption peak at 652 nm compared with that containing Pt/COFs and Pd/COFs, owing to the synergistic effect of bimetallic nanoparticles. In addition, compared with bare COFs, the absorbance intensity increased by 7.81-fold. POD-like and OXD-like activities of Pt–Pd/COFs nanozyme were demonstrated through TMB oxidation process. In addition, the absorbance of system continuously enhanced with the concentration of Pt–Pd/COFs increasing (Fig. 3c), indicating that Pt–Pd/COFs nanozyme possessed intrinsic POD-like activity. As shown in Fig. 3d, in the reaction systems contained only TMB, H_2O_2 or Pt–Pd/COFs, no obvious absorption peaks were observed at 652 nm. In the presence of TMB and Pt–Pd/COFs, an absorption peak at 652 nm was obtained. While a stronger absorption peak was observed in the reaction system that existed both TMB, H_2O_2 and Pt–Pd/COFs. Therefore, the synthesized Pt–Pd/COFs nanozyme

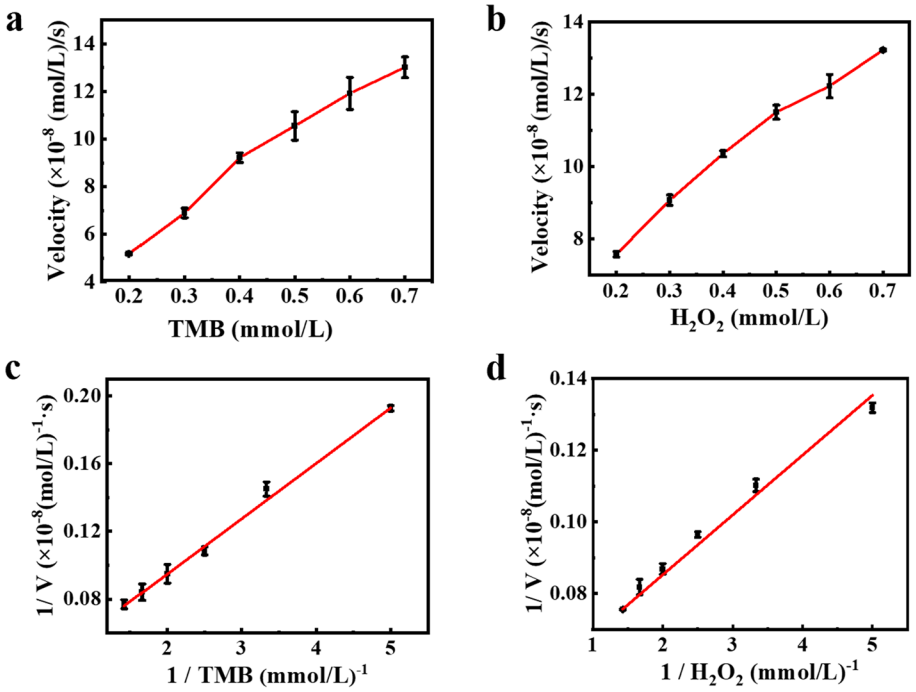

Fig. 2 Michaelis–Menten fitting curves of Pt–Pd/COFs nanozyme with **a** TMB and **b** H_2O_2 as substrates. **c**, **d** Lineweaver–Burk model of **a** and **b**

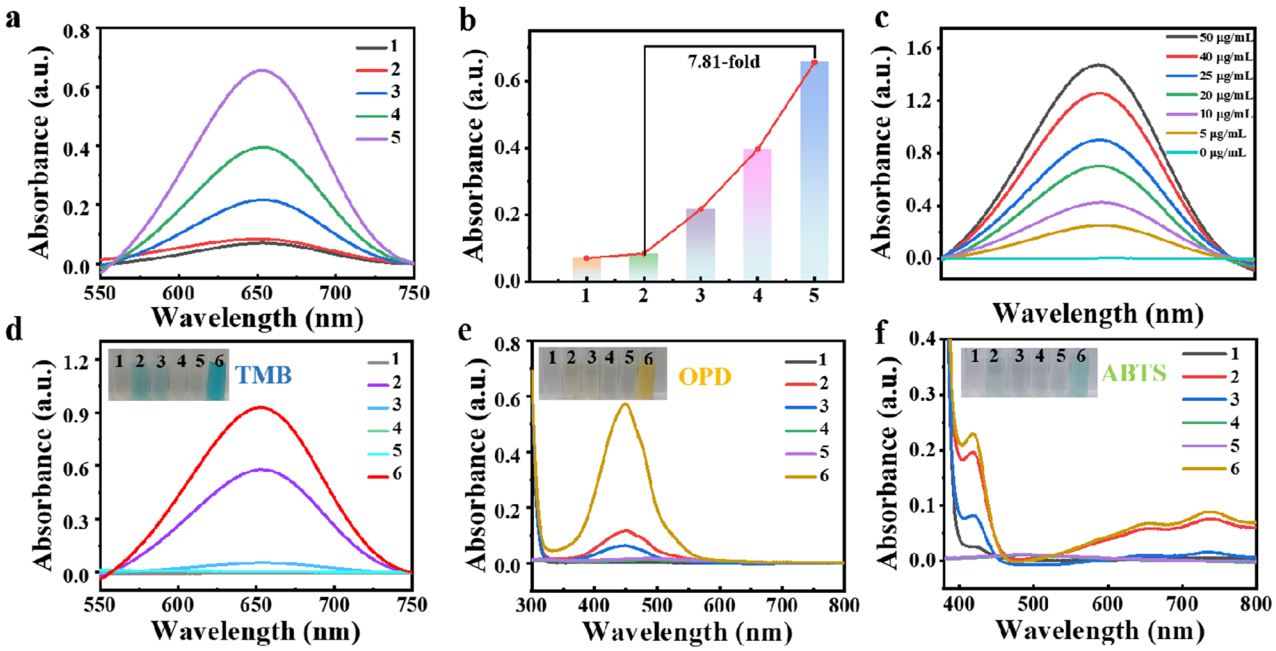

Fig. 3 **a** UV–Vis spectra of various reaction solutions and **b** the corresponding absorption intensity at 652 nm: (1) TMB + H_2O_2, (2) TMB + H_2O_2 + COFs, (3) TMB + H_2O_2 + Pt/COFs, (4) TMB + H_2O_2 + Pd/COFs and (5) TMB + H_2O_2 + Pt–Pd/COFs. **c** Absorption spectra of TMB-H_2O_2 system with different concentrations of Pt–Pd/COFs nanozyme. **d**–**f** The absorption spectra of various reaction systems with various chromogenic substrates (insets: the relevant physical photos) (1) TMB, OPD, or ABTS; (2) TMB, OPD, or ABTS + Pt–Pd/COFs; (3) TMB, OPD, or ABTS + H_2O_2; (4) Pt–Pd/COFs; (5) H_2O_2 + Pt–Pd/COFs; (6) TMB, OPD, or ABTS + H_2O_2 + Pt–Pd/COFs

had the dual enzyme properties of POD-like and OXD-like activities. Subsequently, o-phenylenediamine (OPD) and 2,2′-azino-bis(3-ethylbenzthiazoline-6-sulphonate) (ABTS) were also used as colorimetric substrates to further verify the enzymatic activity of Pt–Pd/COFs nanozyme. As shown in Fig. 3e, f, OPD and ABTS were oxidized by Pt–Pd/COFs nanozyme and the absorption peaks appeared at 448 nm and 416 nm respectively, which further evidenced the POD-like and OXD-like activities of Pt–Pd/COFs nanozyme.

To achieve the optimal catalytic performance of the Pt–Pd/COFs nanozyme, experimental conditions including the pH of the reaction system and the incubation time of GSH were investigated. As shown in Fig. S4, pH 4.5 was the optimal value for TMB oxidation. The rate of catalysis of the Pt–Pd/COFs nanozyme gradually increased with reaction time and reached stable at 20 min, so the optimal incubation time was 20 min for GSH detection (Fig. S5).

The catalytic mechanism of POD-like and OXD-like activities of Pt–Pd/COFs nanozyme were also investigated (Fig. 4a). To confirm the POD-like activity of Pt–Pd/COFs nanozyme, the catalytic mechanism was further investigated in the presence of H_2O_2. Owing to the strong affinity of the Pt–Pd/COFs nanozyme for H_2O_2 (K_m = 0.32 mmol/L), when H_2O_2 was added into the reaction system, H_2O_2 was first adsorbed on the surface of Pt–Pd/COFs nanozyme, after which the O–O bonds in the H_2O_2 broke and decomposed to form ·OH. To confirm the presence of ·OH, PTA was as the specific fluorescent probe, which could absorb ·OH and produce 2-hydroxyterephthalic acid with the high fluorescence intensity at around 425 nm [41]. As shown in Fig. 4b, the fluorescence intensity at 425 nm increased gradually with the increasing time, indicating that Pt–Pd/COFs nanozyme catalyzed H_2O_2 to produce ·OH intermediate continuously. Besides, isopropanol (·OH scavenger agent) was used to validate the formation of ·OH. The A_{652} significantly decreased with the addition of isopropanol into the reaction solution, proving the production of ·OH (Fig. S6). Furthermore, ultra-low electron paramagnetic resonance spectroscopy (EPR) was also utilized to study the generation of ·OH. During the oxidation process of TMB with H_2O_2, the quadruple peak signal with a typical intensity ratio of 1:2:2:1 was presented (Fig. 4c), confirming the generation of ·OH.

To investigate the effect of O_2 on oxidase catalytic activity, the TMB oxidation reactions were carried out in nitrogen, air and oxygen-saturated atmosphere, respectively. The absorbance intensity was that $A_{652}(O_2) > A_{652}(air) > A_{652}(N_2)$ (Fig. 4d). It showed that O_2 participated in the oxidation of TMB. Then, p-benzoquinone (PBQ, $O_2^{\cdot-}$ scavenger) was used to further evaluate the type of reactive oxygen species during the process of TMB oxidation. As shown in Fig. 4e, after the addition of 1 mmol/L PBQ to the Pt–Pd/COFs system, OXD-like activity was significantly inhibited,

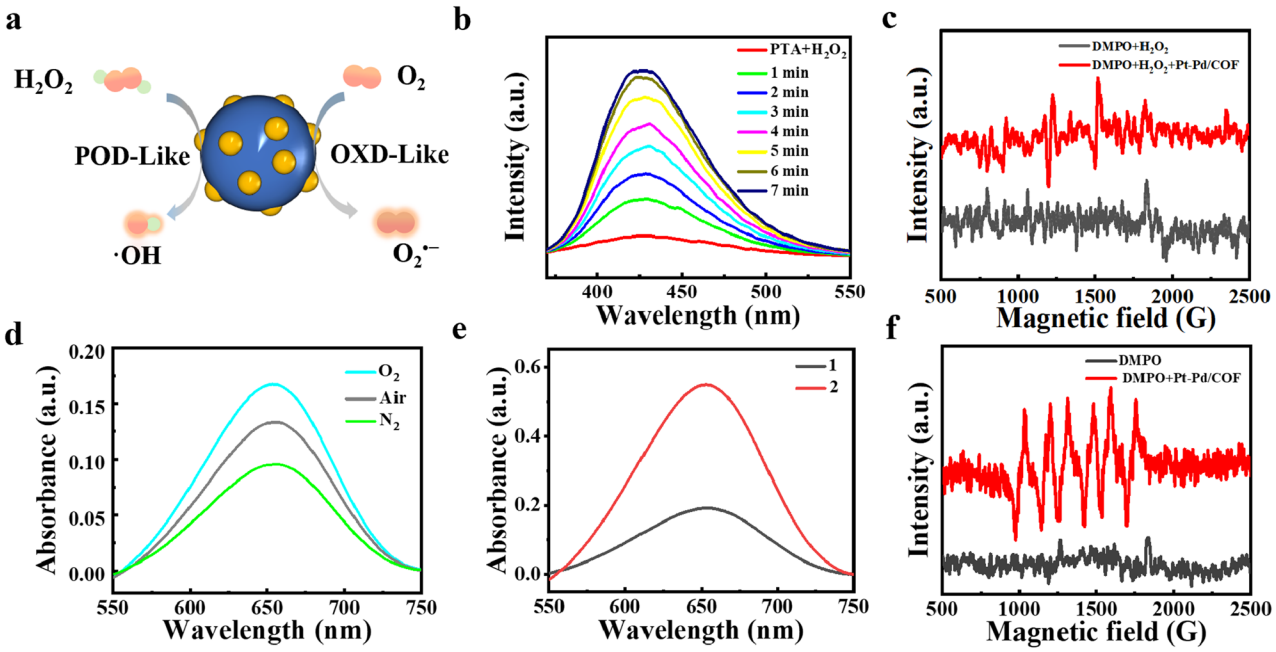

Fig.4 **a** Schematic diagram of POD-like and OXD-like activities of Pt–Pd/COFs nanozyme. **b** Fluorescence spectra of PTA + H_2O_2 + Pt–Pd/COFs reaction systems under different reaction time conditions. **c** EPR spectra of ·OH trapped by DMPO. **d** UV–Vis absorption spectra of Pt–Pd/COFs under different atmospheric conditions: N_2, air and O_2. **e** UV–Vis spectra of various reaction systems: (1) Pt–Pd/COFs + TMB + PBQ and (2) Pt–Pd/COFs + TMB. **f** EPR spectra of $O_2^{\cdot-}$ trapped by DMPO

which showed that $O_2^{\cdot-}$ was generated during TMB oxidation process. In addition, in the reaction system contained 5,5-dimethyl-1-pyrroline N-oxide (DMPO) and Pt–Pd/COFs nanozyme, the quadruple peak with a distinct signal of 1:1:1:1 was also displayed in the EPR spectrum (Fig. 4f), indicating that Pt–Pd/COFs nanozyme could catalyze O_2 to product $O_2^{\cdot-}$. Pt–Pd/COFs nanozyme could capture O_2 molecules and catalyze the cleavage of O–O bonds into $O_2^{\cdot-}$ due to its large specific surface area and porous structure [42]. The dispersed Pt–Pd bimetallic nanoparticles provided enough metal active sites to convert O_2 to $O_2^{\cdot-}$, resulting in the oxidation of TMB. These experimental results proved the Pt–Pd/COFs nanozyme held excellent OXD-like activity.

3.4 Colorimetric Assay of H_2O_2

Based on the POD-like activity of Pt–Pd/COFs nanozyme, a turn-on colorimetric assay was constructed for the detection of H_2O_2 (Fig. 5a). As shown in Fig. 5b, c, with the increasing concentration of H_2O_2, the absorbance intensity at 652 nm increased gradually, and exhibited a good linear relationship in the range of 5–1000 μmol/L. The linear regression equation was $y = 0.0627\ \mathrm{Log}c - 0.0061$ ($R^2 = 0.9977$) and the detection limit was 1.14 μmol/L ($3\sigma/k$). The assay presented in this paper had a lower detection limit than other reported works (Table S1). In addition, we also explored the selectivity of the assay. The interferences including Na^+, K^+, Ca^{2+}, glucose, Al^{3+}, Zn^{2+}, Mg^{2+}, urea and uric acid showed inconspicuous absorbance compared with H_2O_2 (Fig. 5d), which confirmed the good selectivity of the colorimetric assay for the detection of H_2O_2. Moreover, the reproducibility was also verified by five independent parallel experiments, which showed similar absorbance value, implying that the colorimetric assay based on Pt–Pd/COFs nanozyme had good reproducibility for the detection of H_2O_2 (Fig. 5e).

3.5 Colorimetric Assay of GSH

Based on the OXD-like activity of Pt–Pd/COFs nanozyme, a turn-off colorimetric platform was constructed for GSH detection (Fig. 6a). As shown in Fig. 6b, the Pt–Pd/COFs nanozyme catalyzed the TMB–O_2 system to produce a significant absorbance peak, nevertheless the absorbance intensity decreased obviously with the addition of GSH, which was due to the fact that GSH caused the reduction of oxidized-TMB. The A_{652} gradually decreased with the GSH increasing concentration, and exhibited a favorable linear relationship in the concentration range of 1–40 μmol/L (Fig. 6c). The linear regression equation was $y = -0.0121x + 0.6818$ ($R^2 = 0.9942$) and the detection limit for GSH was calculated to be 0.43 μmol/L ($3\sigma/k$) (Fig. 6d). The Pt–Pd/COFs nanozyme-based colorimetric platform exhibited a lower detection limit compared with other detection methods listed in Table S2. The selectivity

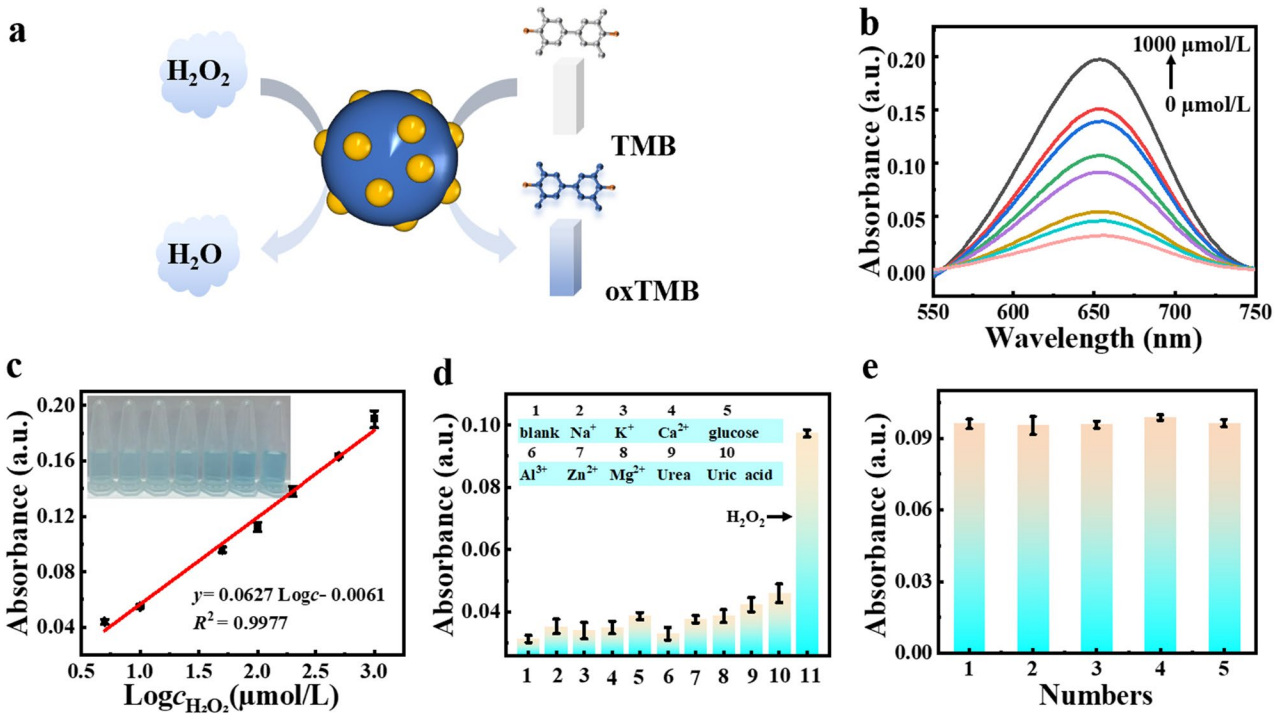

Fig. 5 **a** The schematic illustration of detection principle for H_2O_2. **b** UV–Vis absorption spectra of TMB and Pt–Pd/COFs nanozyme system with various concentrations of H_2O_2. **c** A linear curve at A_{652} with different concentrations of H_2O_2 (Inset: the color change with increasing concentrations of H_2O_2). **d**, **e** Selectivity and reproducibility experiments for H_2O_2 sensing

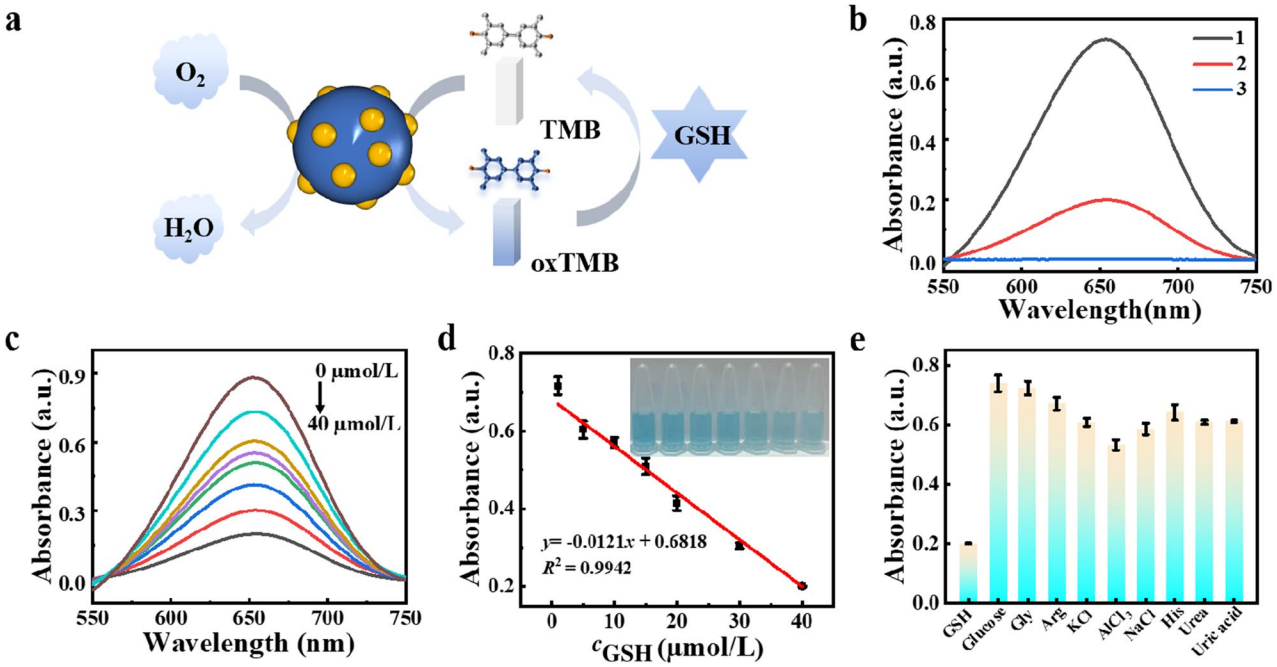

Fig. 6 **a** The schematic illustration of detection principle for GSH. **b** UV–Vis absorption spectra of various reaction systems: (1) TMB + Pt–Pd/COFs, (2)TMB + Pt–Pd/COFs + GSH and (3) TMB. **c** UV–Vis absorption spectra of TMB and Pt–Pd/COFs nanozyme system with various concentrations of GSH. **d** A linear curve at A_{652} with different concentrations of GSH (inset: the color change with increasing concentrations of GSH). **e** Selectivity experiments for GSH sensing

of Pt–Pd/COFs nanozyme for GSH detection was investigated (Fig. 6e). Compared with a variety of interfering substrates, including glucose, glycine (Gly), arginine (Arg), K^+, Al^{3+}, Na^+, histidine (His), urea and uric acid, the presence of GSH caused a noticeable decrease of the absorbance intensity, confirming the desirable selectivity of the colorimetric platform for GSH detection. In addition, five independent parallel experiments showed similar absorbance value, implying that the colorimetric assay based on Pt–Pd/COFs nanozyme had good reproducibility for GSH detection (Fig. S7). The stability of Pt–Pd/COFs nanozyme was further evaluated, which still showed good catalytic performance for H_2O_2 and GSH detection after 10 days storage, indicating the good stability of Pt–Pd/COFs nanozyme (Fig. S8).

To verify the feasibility of Pt–Pd/COFs nanozyme in biological applications, the recovery measurements were carried out. As shown in Table S3, the recoveries of H_2O_2 in environmental water were 94.91–108.0%, with the relative standard deviation (RSD) of 2.1–4.3% ($n = 3$). As shown in Table S4, the recoveries of GSH in human serum were 93.70–102.8%, with the RSD of 1.3–2.0% for GSH ($n = 3$). The results indicated the promising applications of the Pt–Pd/COFs nanozyme for H_2O_2 and GSH detection in complex samples.

4 Conclusions

In this study, a multifunctional Pt–Pd/COFs nanozyme simultaneously with superior POD-like activity and OXD-like activity was designed for colorimetric detection of H_2O_2 and GSH. Compared with monometallic nanozyme, the Pt–Pd/COFs nanozyme exhibited higher catalytic activity due to the bimetallic synergistic effect. Using the multifunctional nanozyme, the colorimetric platform realized sensitive detection of H_2O_2 and GSH, with the detection limits of 1.14 μmol/L and 0.43 μmol/L, respectively. The Pt–Pd/COFs nanozyme with dual enzyme-like activities possessed bright prospects in various fields including environmental protection and biosensing.

Supplementary Information The online version contains supplementary material available at https://doi.org/10.1007/s41664-024-00298-y.

Acknowledgements This work was financially supported by the National Natural Science Foundation of China (22076041, 22076042) and the Key Research and Development Program of Hubei Province, China (2023BAB134).

Data Availability The data is available upon reasonable request.

Declarations

Conflict of interest The authors declare that they have no interests.

References

1. Wu JX, Wang XY, Wang Q, Lou ZP, Li SR, Zhu YY, Qin L, Wei H. Nanomaterials with enzyme-like characteristics (nanozymes): next-generation artificial enzymes. Chem Soc Rev. 2019;48:1004–76.
2. Filizola M, Loew GH. Role of protein environment in horseradish peroxidase compound I formation: molecular dynamics simulations of horseradish peroxidase−HOOH complex. J Am Chem Soc. 2000;122(1):18–25.
3. An MY, He MQ, Lin CS, Wu YB, Ai YJ, Xin HB, Liang QL. Recent progress of nanozymes with different spatial dimensions for bioanalysis. Mater Today Nano. 2023;22:100330.
4. Lin YY, Ren JS, Qu XG. Catalytically active nanomaterials: a promising candidate for artificial enzymes. Acc Chem Res. 2014;47(4):1097–105.
5. Chen QM, Liang CH, Zhang XD. High oxidase-mimic activity of Fe nano-particles embedded in an N-rich porous carbon and their application for sensing of dopamine. Talanta. 2018;182:476–83.
6. Liu H, Ding YN, Bian B, Li L, Li RM. Rapid colorimetric determination of dopamine based on the inhibition of the peroxidase mimicking activity of platinum loaded $CoSn(OH)_6$ nanocubes. Microchim Acta. 2019;186:755.
7. Gao LZ, Zhuang J, Nie L, Zhang JB, Zhang Y, Gu N, Wang TH, Feng J, Yang DL, Perrett S, Yan XY. Intrinsic peroxidase-like activity of ferromagnetic nanoparticles. Nat Nanotechnol. 2007;2:577–83.
8. Mu JS, Zhang L, Zhao M, Wang Y. Catalase mimic property of Co_3O_4 nanomaterials with different morphology and its application as a calcium sensor. ACS Appl Mater Interfaces. 2014;6(10):7090–8.
9. Wang XL, Yang Q, Cao YX, Hao HB, Zhao JH, Hao JC. Metallosurfactant ionogels in imidazolium and protic ionic liquids as precursors to synthesize nanoceria as catalase mimetics for the catalytic decomposition of H_2O_2. Chem Eur J. 2016;22(49):17857–65.
10. Natalio F, Andre R, Hartog AF, Stoll B, Jochum KP, Wever R, Tremel W. Vanadium pentoxide nanoparticles mimic vanadium haloperoxidases and thwart biofilm formation. Nat Nanotechnol. 2012;7:530–5.
11. Xi XX, Wang JH, Wang YZ, Xiang HY, Chen MM, Wu Z, Zhang XH, Wang SF, Wen W. Preparation of Au/Pt/$Ti_3C_2Cl_2$ nanoflakes with self-reducing method for colorimetric detection of glutathione and intracellular sensing of hydrogen peroxide. Carbon. 2022;197:476–84.
12. Ye QY, Dai T, Shen J, Xu Q, Hu XY, Shu Y. Incorporation of fluorescent carbon quantum dots into metal–organic frameworks with peroxidase-mimicking activity for high-performance ratiometric fluorescent biosensing. J Anal Test. 2023;7:16–24.
13. Li S, Wei ZY, Xiong L, Xu Q, Yu L, Xiao YX. In situ formation of o-phenylenediamine cascade polymers mediated by metal-organic framework nanozymes for fluorescent and photothermal dual-mode assay of acetylcholinesterase activity. Anal Chem. 2022;94(49):17263–71.
14. Dai XH, Liu H, Cai B, Liu Y, Song KP, Chen J, Ni SQ, Kong LS, Zhan JH. A bioinspired atomically thin nanodot supported single-atom nanozyme for antibacterial textile coating. Small. 2023;19(47):2303901.

15. Wu SL, Wu WW, Zhu XY, Li MH, Zhao JG, Dong SJ. Atomically dispersed hierarchically ordered porous Fe–N–C single-atom nanozymes for dyes degradation. Nano Res. 2023;16:10840–7.
16. Chen JQ, Liu XY, Zheng GZ, Fang W, Wang P, Gao J, Liu JB, Wang MZ, Wang QY. Detection of glucose based on noble metal nanozymes: mechanism, activity regulation, and enantioselective recognition. Small. 2022;19(8):2205924.
17. Cai SF, Duan HH, Liang XX, Wang C, Yang R, Li YD. Single-layer Rh nanosheets with ultrahigh peroxidase-like activity for colorimetric biosensing. Nano Res. 2018;11:6304–16.
18. Dong C, Yu Q, Ye RP, Su PP, Liu J, Wang GH. Hollow carbon sphere nanoreactors loaded with PdCu nanoparticles: void-confinement effects in liquid-phase hydrogenations. Angew Chem Int Ed. 2020;59(42):18374–9.
19. Liu YY, He Q, Li YR, Li YQ, He CY. Synthesis of copper-based nanoparticles confined in a pyridine N-containing COF and their catalytic applications. Micropor Mesopor Mater. 2024;364:112868.
20. Qian C, Teo WL, Gao Q, Wu HW, Liao YZ, Zhao YL. Polycrystalline covalent organic frameworks. Mater Today. 2023;71:91–107.
21. Wang XR, Han X, Zhang J, Wu XW, Liu Y, Cui Y. Homochiral 2D porous covalent organic frameworks for heterogeneous asymmetric catalysis. J Am Chem Soc. 2016;138(38):12332–5.
22. Nguyen HL, Gropp C, Ma YH, Zhu CH, Yaghi OM. 3D covalent organic frameworks selectively crystallized through conformational design, and functions. J Am Chem Soc. 2020;142(48):20335–9.
23. Zhang M, Meng L, Yang MY, Liao JP, Liu YF, Yan HJ, Chang JN, Yu TY, Li SL, Lan YQ. Ultrafine Cu nanoclusters confined within covalent organic frameworks for efficient electroreduction of CO_2 to CH_4 by synergistic strategy. eScience. 2023;3(3):100116.
24. Xin Y, Liu XJ, Wang CL, Liu NZ, Jiang QT, Duan JZ. Electrochemical detection of copper ions with covalent organic frame material modified carbon paste electrode. Chin J Anal Lab. 2023;42(9):1199–204.
25. Liu XY, Wang F, Meng Y, Zhao LP, Shi WJ, Wang X, He ZK, Chao J, Li CL. Electrochemical/visual microfluidic detection with a covalent organic framework supported platinum nanozyme-based device for early diagnosis of pheochromocytoma. Biosens Bioelectron. 2022;207:114208.
26. Yuan RR, Li HK, He HM. Recent advances in metal/covalent organic framework-based electrochemical aptasensors for biosensing applications. Dalton Trans. 2021;50:14091–104.
27. Li GR, Wu YJ, Zhong C, Yang YX, Lin ZA. Predesigned covalent organic framework with sulfur coordination: anchoring Au nanoparticles for sensitive colorimetric detection of Hg(II). Chin Chem Lett. 2023. https://doi.org/10.1016/j.cclet.2023.108904.
28. Zhang C, Wang P, Yin X, Liu H, Yang Y, Cheng L, Song G, Zhang X. Two-photon supramolecular nanoplatform for ratiometric bioimaging. Anal Chem. 2019;91(9):6371–7.
29. Lai X, Shen Y, Gao SB, Chen YJ, Cui YS, Ning DX, Ji XB, Liu ZW, Wang LG. The Mn-modified porphyrin metal-organic framework with enhanced oxidase-like activity for sensitively colorimetric detection of glutathione. Biosens Bioelectron. 2022;213:114446.
30. Li G, Hu GX, Chen B, Gu Y, Yang JY, Yang HB, Hu FX, Li CM, Guo CX. Boosting photo-electro-fenton process via atomically dispersed iron sites on graphdiyne for in vitro hydrogen peroxide detection. Small. 2023;19(33):2301540.
31. Zhu ZM, Yan DP, Huang ZH, Zhong XL, Shen Y. Detection of glutathione based on nitrogen-doped carbon dots as a fluorescence probe. Chin J Anal Lab. 2023;42(11):1508–15.
32. Ganganboina AB, Doong R. The biomimic oxidase activity of layered V_2O nanozyme for rapid and sensitive nanomolar detection of glutathione. Sens Actuators B Chem. 2018;273:1179–86.
33. Li JZ, Li YH, Gao ZF. Polydopamine-based colorimetric superwettable biosensor for highly sensitive detection of hydrogen peroxide and glucose. J Anal Test. 2023;7:118–27.
34. Liang Y, Liu YY, Zhao P, Chen YY, Lei JC, Hou JZ, Hou CJ, Hou DQ. An electrochemical sensor based on FeCo bimetallic single-atom nanozyme for sensitive detection of H_2O_2. Anal Chim Acta. 2023;1281:341867.
35. Liang N, Ge XY, Zhao Y, Xia L, Song ZL, Kong RM, Qu FL. Promoting sensitive colorimetric detection of hydroquinone and Hg^{2+} via ZIF-8 dispersion enhanced oxidase-mimicking activity of MnO_2 nanozyme. J Hazard Mater. 2023;454:131455.
36. Wang HS, Wu FL, Wu LF, Guan JQ, Niu XD. Nanozyme colorimetric sensor array based on monatomic cobalt for the discrimination of sulfur-containing metal salts. J Hazard Mater. 2023;456:131643.
37. Feng SN, Yan MX, Xue Y, Huang JS, Yang XR. Electrochemical immunosensor for cardiac troponin I detection based on covalent organic framework and enzyme-catalyzed signal amplification. Anal Chem. 2021;93(40):13572–9.
38. Peng XL, Zhu JL, Wu Z, Wen W, Zhang XH, Chen MM, Wang SF. High-efficient Pt@COF nanospheres-based electrochemical-chemical-chemical redox cycling for ultrasensitive microRNAs biosensing. Sens Actuators B Chem. 2023;392:134074.
39. Zhang T, Chen YL, Huang W, Wang Y, Hu XY. A novel AuNPs-doped COFs composite as electrochemical probe for chlorogenic acid detection with enhanced sensitivity and stability. Sens Actuators B Chem. 2018;276:362–9.
40. Kang X, Cao GJ, Wang JP, Wang J, Zhu X, Fu MY, Yu DH, Hua L, Gao FL. Synergistic action of cavity and catalytic sites in etched Pd-Cu_2O octahedra to augment the peroxidase-like activity of Cu_2O nanoparticles for the colorimetric detection of isoniazid and ascorbic acid. Biosens Bioelectron. 2024;246:115880.
41. Zhou LL, Guan Q, Li YA, Zhou Y, Xin YB, Dong YB. One-pot synthetic approach toward porphyrinatozinc and heavy-atom involved Zr-NMOF and its application in photodynamic therapy. Inorg Chem. 2018;57(6):3169–76.
42. Zhuang YX, Zhang XD, Chen QM, Li SQ, Cao HY, Huang YM. Co_3O_4/CuO hollow nanocage hybrids with high oxidase-like activity for biosensing of dopamine. Biomater Adv. 2019;94:858–66.